PHYSICAL REVIEW E **88**, 041101(R) (2013)

Scaling laws for ignition at the National Ignition Facility from first principles

Baolian Cheng,* Thomas J. T. Kwan, Yi-Ming Wang, and Steven H. Batha
Los Alamos National Laboratory, Los Alamos, New Mexico 87545, USA
(Received 3 May 2013; published 7 October 2013)

We have developed an analytical physics model from fundamental physics principles and used the reduced one-dimensional model to derive a thermonuclear ignition criterion and implosion energy scaling laws applicable to inertial confinement fusion capsules. The scaling laws relate the fuel pressure and the minimum implosion energy required for ignition to the peak implosion velocity and the equation of state of the pusher and the hot fuel. When a specific low-entropy adiabat path is used for the cold fuel, our scaling laws recover the ignition threshold factor dependence on the implosion velocity, but when a high-entropy adiabat path is chosen, the model agrees with recent measurements.

DOI: 10.1103/PhysRevE.88.041101 PACS number(s): 52.57.−z, 52.50.Lp

Inertial confinement fusion (ICF) ignition experiments at the National Ignition Facility (NIF) are guided by the ignition threshold factor (ITF) [1], which characterizes the probability of ignition as a function of implosion velocity ($V_{\rm imp}$), fuel adiabat (α), fuel mass, and hydrodynamic mixing. The factor is normalized so that a value of 1.0 represents a 50% probability of ignition, the point at which the expected shell kinetic energy exactly equals the minimum implosion energy required for ignition. The particular form of the ITF is central to establishing the driver requirements for inertial confinement fusion and is also of considerable interest in the optimization of an inertial fusion driver design. The ITF used in the National Ignition Campaign (NIC) was obtained by fitting the results of a series of numerical simulations performed for a certain subset of imploding fuel configurations [2]. Recent NIC experimental results [3] show that although the peak implosion velocity reached over 90% of the value predicted to be necessary for ignition, the neutron yields of the capsules were still two to three orders of magnitude from ignition and a factor of 10 below the code predictions. The inferred energy in the fuel hot spot was only 1/7th of the total energy in the capsule, and the measured aspect ratio (the ratio of the thickness Δ_p of the cold fuel to the radius $R_{\rm hs}$ of the hot spot) was 0.7 ± 0.05 [3] compared to the calculated energy ratio of 1/3 and aspect ratio of 1.15 ± 0.05 derived from code simulations [4].

In this Rapid Communication, we formulate the ITF from first principles, beginning with a reduced one-dimensional (1D) fundamental physics model to derive analytically a thermonuclear ignition criterion and implosion energy-scaling laws applicable to ICF capsules. Such a reduced-physics model will help to identify possible inadequate assumptions and improve modeling of the experiments.

The necessary and sufficient condition for achieving ignition in NIF capsules is to have a sustainable thermonuclear burn of the hot spot deuterium-tritium (DT) fuel. Ignition requires that the fusion reaction reproduction time ($\tau_{\rm rep} = E_T/\dot{E}$) be shorter than the hydrodynamic disassembly time ($\tau_H = R_{\rm hs}/C_s$),[1] where $E_T = 2 \times (3/2)(n_{\rm D} + n_{\rm T})kT + E_{\rm rad}$ is the total energy density of the hot fuel, k the Boltzmann constant, $E_{\rm rad}$ the radiation energy density, $\dot{E} = n_{\rm T} n_{\rm D} \langle \sigma v \rangle_{\rm DT} W_\alpha$ the energy deposition rate by fusion reactions, W_α the energy deposited into the hot DT per fusion, which normally equals a fraction (f_α) of the α-particle energy (~3.52 MeV), and C_s the sound speed. Such a condition results in a threshold on the areal density of the hot DT fuel,

$$(\rho R)_{\rm hs} \geqslant \frac{(1+d)^2}{d} \frac{[3kT + E_{\rm rad}/n] C_s A_{\rm DT}}{\langle \sigma v \rangle_{\rm DT} W_\alpha N_A}, \qquad (1)$$

where we neglected the energy loss by other forms, e.g., bremsstrahling radiation, heat conduction, etc. $A_{\rm DT}$ is the atomic mass number of the DT mixture, N_A the Avogadro's number, and $n = n_{\rm D} + n_{\rm T}$ the total number density of the ions. This threshold depends on the ratio of D to T ($d \equiv n_{\rm D}/n_{\rm T}$), nuclear reactivity $\langle \sigma v \rangle_{\rm DT}$, and fuel temperature. In high-density hot DT fuel, the matter energy dominates over the radiation energy. For simplicity, the radiation term on the hot spot is ignored throughout the analysis. In this work we focus on $d = 1$ and $f_\alpha = 1$, which correspond to the most optimum condition for ignition. For a temperature range of 3–6 keV, using a power law approximation $\langle \sigma v \rangle_{\rm DT} \sim T^4$, the ignition condition reduces to $(\rho R)_{\rm hs} \geqslant 4\kappa (T/{\rm keV})^{-2.5}$ g/cm^2, where $\kappa = 3.776/f_T$ is a numerical constant. A detailed analysis of this ignition criterion will be presented in a separate paper. The goal of this Rapid Communication is to find the minimum implosion energy necessary for the hot DT fuel to achieve ignition.

Implosion delivers the required energy to the system. For a short-pulse radiation-driven system, such as NIF, we can assume that the maximum implosion energy is achieved at the peak implosion velocity time and equals the peak pusher kinetic energy. We now introduce a physics model for a typical capsule consisting of a "pusher" and hot DT fuel. The pusher here represents the sum of the remaining ablator and the cold DT fuel. Applying the energy conservation law to the capsule at the $V_{\rm imp}$ time and assuming that all the implosion energy

*bcheng@lanl.gov

[1]To account for the tamping effect, C_s becomes the effective sound speed $C_s^* = C_s/f_T$, where $f_T \propto \sqrt{\rho_p/\rho_{\rm hs}}$ is a tamping factor. Here ρ_p and $\rho_{\rm hs}$ are the mass density of the pusher and the hot spot at the interface, respectively. If the interface between the hot spot and pusher is not sharp, the tamping factor is decreased. The NIC burn width data suggest $f_T \sim 1.8$–2.0 for NIC capsules.

is converted into the internal energy of the capsule at ignition time,

$$\tfrac{1}{2}\eta M_p V_{\rm imp}^2 = \epsilon_p M_p + \epsilon_{\rm hs} M_{\rm hs}, \tag{2}$$

where M_p and $M_{\rm hs}$ are the masses of the pusher and hot spot, respectively, ϵ_p ($\epsilon_{\rm hs}$) the specific internal energy of the pusher (hot spot DT), and $\eta \leqslant 1$ a coefficient accounting for the possible energy losses from the system during the implosion process, for example, rotational energy of the shell, etc. We assume a gamma law for cold DT, $P/P_0 = (\rho/\rho_0)^{\gamma_p}$ and $\epsilon_p = \epsilon_0 (P/P_0)^{\frac{\gamma_p - 1}{\gamma_p}}$, where P_0, ρ_0, and ϵ_0 are, respectively, the pressure, mass density, and specific internal energy of the pusher at the peak implosion time, and γ_p the adiabat index of the pusher. For hot DT fuel, $P = 2\rho_{\rm hs} RT/A_{\rm DT}$, $\epsilon_{\rm hs} = 2RT/[A_{\rm DT}(\gamma_g - 1)]$, where R is the gas constant and γ_g the adiabat index of the hot DT. Assuming the fuel and pusher are in pressure equilibrium at the stagnation time, from Eq. (1) the mass of the pusher can be expressed in terms of the fuel pressure

$$M_p = \frac{\frac{4\pi}{3}(\rho_{\rm hs} R_{\rm hs})^3 \epsilon_{\rm hs} \left(\frac{2N_A kT}{A_{\rm DT} P_0}\right)^2}{\left[\eta V_{\rm imp}^2/2 - \epsilon_0 (P/P_0)^{\frac{\gamma_p - 1}{\gamma_p}}\right](P/P_0)^2}. \tag{3}$$

This parameter is critical in capsule design because of the dual roles of the pusher, which not only delivers the total energy to the system through its kinetic energy, but also is a sink, sharing the energy with the hot fuel through its internal energy. Thus, for a given implosion velocity, and for now disregarding instabilities in the ICF capsule, there is an optimum balance between the pusher energy and the hot fuel energy or the mass ratio of the cold fuel to the hot spot. Applying the least-energy principle, and minimizing the mass of the pusher for given $V_{\rm imp}$ with respect to the fuel pressure for fixed ignition condition (1), yields

$$\frac{P}{P_0} = \left[\frac{\gamma_p}{(3\gamma_p - 1)\epsilon_0}\eta V_{\rm imp}^2\right]^{\frac{\gamma_p}{\gamma_p - 1}}, \tag{4}$$

which shows the dependence and sensitivity of the hot fuel pressure on implosion velocity and the equation of state (EOS) of the pusher. Taking $\gamma_p = 3$, Eq. (4) recovers the scaling law $P \propto V_{\rm imp}^3$ demonstrated in the code simulations and adopted in the ITF.[2] If we take $\gamma_p = 5/3$, as in an ideal gas, Eq. (4) produces a scaling law $P \propto V_{\rm imp}^5$. Physically, at the same compression, a gas with $\gamma_p = 3$ would result in higher pressures compared with $\gamma_p = 5/3$ because $\gamma_p \propto \ln P/\ln \rho$. Figure 1 shows the two scaling laws plotted against the NIC data. Our scaling law fits the data better (in curvature) than does the current scaling law. We can evaluate the model against the NIC experimental data by first using scaling law (4) to derive the following physical quantities: (1) mass ratio $M_{\rm hs}/M_p$, (2) areal density ratios $(\rho R)_{\rm hs}/(\rho R)_p$ and $(\rho R)_{\rm hs}/(\rho R)_{\rm tot}$, (3) volume ratio $V_{\rm hs}/V_p$, (4) aspect ratio $\Delta_p/R_{\rm hs}$, (5) energy ratios $E_{\rm hs}/E_p$ and $E_{\rm hs}/E_{\rm tot}$, (6) mass density ratio $\rho_{\rm hs}/\rho_p$, (7) hot spot pressure $P_{\rm hs}$, and (8) neutron yield. These

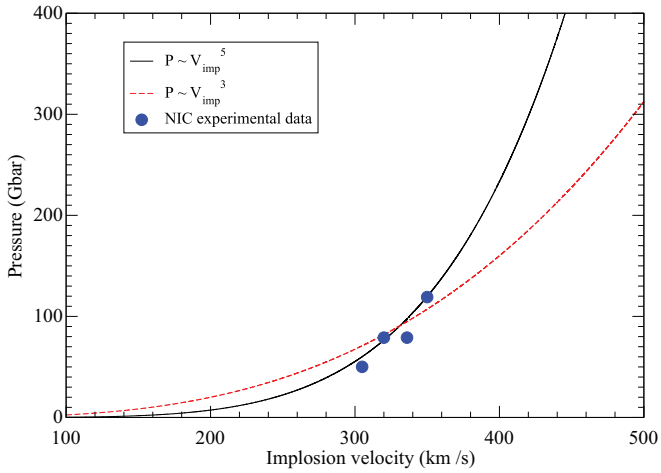

FIG. 1. (Color online) The observed NIC data plotted against scaling laws $P \propto V_{\rm imp}^3$ and $P \propto V_{\rm imp}^5$, respectively. The top right data point is from shot No. N110914.

quantities are obtained in terms of measurable parameters as follows:

$$\frac{M_{\rm hs}}{M_p} = \frac{(\gamma_p - 1)\eta V_{\rm imp}^2}{(3\gamma_p - 1)2\epsilon_{\rm hs}}, \tag{5}$$

$$\frac{(\rho R)_{\rm hs}}{(\rho R)_p} = \left[\left(1 + \frac{2\gamma_p}{\gamma_g - 1}\right)^{1/3} + \left(1 + \frac{2\gamma_p}{\gamma_g - 1}\right)^{2/3} + 1\right]\frac{M_{\rm hs}}{M_p}, \tag{6}$$

$$\frac{(\rho R)_{\rm hs}}{(\rho R)_{\rm tot}} = \frac{(\rho R)_{\rm hs}/(\rho R)_p}{1 + (\rho R)_{\rm hs}/(\rho R)_p}, \tag{7}$$

$$\frac{V_{\rm hs}}{V_p} = \frac{\gamma_g - 1}{2\gamma_p}, \quad \frac{\Delta_p}{R_{\rm hs}} = \left[1 + \frac{2\gamma_p}{\gamma_g - 1}\right]^{1/3} - 1, \tag{8}$$

$$\frac{E_{\rm hs}}{E_p} = \frac{\gamma_p - 1}{2\gamma_p}, \quad \frac{E_{\rm hs}}{E_{\rm tot}} = \frac{\gamma_p - 1}{3\gamma_p - 1}, \tag{9}$$

$$\frac{\rho_{\rm hs}}{\rho_p} = \frac{2\gamma_p}{(\gamma_g - 1)}\frac{M_{\rm hs}}{M_p} = [(1 + \Delta_p/R_{\rm hs})^3 - 1]\frac{M_{\rm hs}}{M_p}, \tag{10}$$

$$P_{\rm hs} = 2\frac{(\rho R)_{\rm hs} RT}{A_{\rm DT} R_{\rm hs}}, \tag{11}$$

$$Y_n = 2.27 \times 10^4 \frac{f_T}{2}\frac{(\gamma_p - 1)(\gamma_g - 1)}{(3\gamma_p - 1)\sqrt{\gamma_g}} M_p \eta V_{\rm imp}^2 T^{2.5} (\rho R)_{\rm hs}, \tag{12}$$

where M_p is in g, $V_{\rm imp}$ in km/s, and T in keV. The aspect ratio of the capsules was directly measured [3] and can be used to estimate the ratio of the hot fuel energy to the total implosion energy,

$$\frac{E_{\rm hs}}{E_{\rm tot}} = \frac{(\gamma_g - 1)[(1 + \Delta_p/R_{\rm hs})^3 - 1]/2 - 1}{3(\gamma_g - 1)[(1 + \Delta_p/R_{\rm hs})^3 - 1]/2 - 1},$$

and a range for the adiabat index of the pusher in the experiments,

$$\gamma_p = \frac{(\gamma_g - 1)}{2}[(1 + \Delta_p/R_{\rm hs})^3 - 1].$$

[2]Note that the code calculations did not actually use $\gamma_p = 3$, however, this analysis shows that the results from the code calculations are consistent with the results setting $\gamma_p = 3$ in this model.

TABLE I. Comparison among theory, data, and simulations. In the table, $\nu \equiv \eta A_{\rm DT} V_{\rm imp}^2/2RT$.

Adiabat index	Theory			NIC data	Codes
	$\gamma_p = 4/3$	$\gamma_p = 5/3$	$\gamma_p = 3$		$\alpha \approx 1.65$
$\Delta_p/R_{\rm hs}$	0.71	0.816	1.153	0.66–0.85	1.1–1.2
$E_{\rm hs}/E_p$	1/8	1/5	1/3	0.15–0.2	0.4–0.6
$E_{\rm hs}/E_{\rm tot}$	1/9	1/6	1/4	0.12	0.3
$V_{\rm hs}/V_p$	1/4	1/5	1/9	0.215	0.11
$M_{\rm hs}/M_p$	$\nu/27$	$\nu/18$	$\nu/12$	0.025	0.082
$(\rho R)_{\rm hs}/(\rho R)_p$	0.21ν	0.34ν	0.65ν		0.29
$\rho_{\rm hs}/\rho_p$	0.148ν	0.28ν	0.75ν		
$(\rho R)_{\rm tot}/(\rho R)_{\rm hs}$	$4.76/\nu + 1$	$2.94/\nu + 1$	$1.54/\nu + 1$		

As shown above, the mass and areal density ratios of the hot spot to the pusher and the hot spot pressure are determined not only by the implosion velocity but also by the EOSs of the cold and hot fuel. But the volume, energy, and aspect ratios are purely determined by the EOSs of the cold and hot DT. Table I compares the model predictions using $\gamma_g = 5/3$ at three different values of γ_p with both NIC data and simulations. The analytical model is consistent with the experimental data when γ_p values of 4/3–5/3 are used and agree with the numerical simulations at $\gamma_p \simeq 3$. This implies that at the peak implosion velocity time, the pushers in the NIC capsules may have actually been shocked or preheated to a higher entropy adiabat than expected. For a more detailed comparison, we take shot No. N120321 [3,4] as an example. In N120321, $T_i \simeq 3.06$ keV, $V_{\rm imp} \simeq 315$ km/s, and $\nu = 0.42$ for $\eta = 1$. Table II compares the model predictions of the various physical quantities with the experimental data and postshot simulations for N120321. Comparisons show that the model predictions agree with the N120321 data at $\gamma_p = 4/3$ and the simulations at $\gamma_p = 3$. Furthermore, as shown in Fig. 2, plotting the ratios of mass, volume, and energy versus the aspect ratio of the capsule in the NIC experiments, the model with a high-entropy pusher adiabat ($\gamma_p \simeq 4/3$–$5/3$) again consistently agrees with the NIC data while the model with a low-entropy adiabat ($\gamma_p \simeq 2$–3) better fits the code calculations.

From Eqs. (3) and (4), we obtain the minimum required implosion energy for a given implosion velocity,

$$E^{\rm min} = \frac{4\pi}{3}(\rho_{\rm hs} R_{\rm hs})^3 \epsilon_{\rm hs} \left(\frac{2N_A k T_{\rm ign}}{A_{\rm DT} P_0}\right)^2 \left(\frac{3\gamma_p - 1}{\gamma_p - 1}\right) \times \left(\frac{\eta\gamma_p/\epsilon_0}{3\gamma_p - 1}\right)^{-\frac{2\gamma_p}{\gamma_p - 1}} V_{\rm imp}^{-\frac{4\gamma_p}{\gamma_p - 1}}, \quad (13)$$

where $T_{\rm ign}$ is the ignition temperature specified by Eq. (1). For $\gamma_p = 3$, $E^{\rm min} \propto V_{\rm imp}^{-6}$, which is the scaling law demonstrated in the simulations and adopted in the ITF formulation [1]. If $\gamma_p = 5/3$, scaling law becomes $E^{\rm min} \propto V_{\rm imp}^{-10}$. Within the framework of this model, this implies that a tiny change of implosion velocity would require the implosion energy $E^{\rm min}$ for $\gamma_p = 5/3$ to change more rapidly than that for $\gamma_p = 3$. In other words, our derived minimum implosion energy for ignition is significantly sensitive to both the pusher EOS and the implosion velocity. The experimental data also suggest that the required minimum implosion energy is more sensitive to the implosion velocity than the ITF suggests.

To achieve ignition, the implosion energy must satisfy both conditions $\eta M_p V_{\rm imp}^2/2 \geqslant E^{\rm min}$ and $(\rho R)_{\rm hs} \geqslant 4\kappa T^{-2.5}$. This generates the required condition for the implosion energy and the energy-scaling law, ITF. However, in practice, instabilities developed from implosion asymmetry and the roughness of

TABLE II. Comparison among theory, data, and simulations for shot No. N120321. In the table, DSR $\equiv (\rho R)_{\rm tot}/21$ is the neutron downscattered ratio. A comparison shows that the model predictions agree with the N120321 data at $\gamma_p = 4/3$.

Adiabat index	Theory			N120321 data	Codes
	$\gamma_p = 4/3$	$\gamma_p = 5/3$	$\gamma_p = 3$		$\alpha \approx 1.65$
$E_{\rm hs}/E_p$	0.125	0.2	0.333	0.18	0.55
$E_{\rm hs}/E_{\rm tot}$	0.11	0.167	0.25	0.10	0.30
$\Delta_p/R_{\rm hs}$	0.71	0.816	1.153	0.72	1.18
$V_{\rm hs}/V_p$	0.25	0.2	0.11		
$M_{\rm hs}/M_p$	0.027	0.041	0.063	0.025	0.081
$(\rho R)_{\rm hs}/(\rho R)_p$	0.158	0.255	0.49		0.282
$(\rho R)_{\rm hs}/(\rho R)_{\rm tot}$	0.136	0.20	0.328	0.055	0.272
$\rho_{\rm hs}/\rho_p$	0.115	0.218	0.58		0.19
DSR	0.0614	0.0614	0.0614	0.062 58	0.0622
$P_{\rm hs}$ (Gbar)	107	165	283	110	256
Y_n (10^{14})	4.36	10.15	26	4.16	24

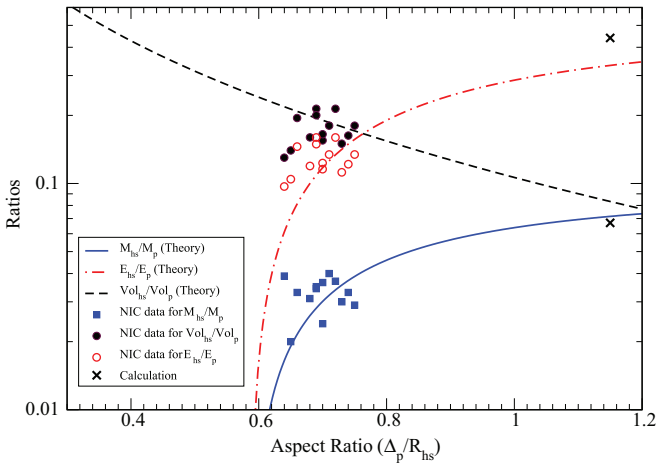

FIG. 2. (Color online) Comparison among theory, experimental data, and code simulations. The x axis is the aspect ratio of the capsule at the ignition time. The NIC data agree with the theory at a high-entropy adiabat of the pusher, while the code calculations correspond to a low-entropy adiabat of the pusher.

the interface between the cold and hot DT gas would lead to mixing of the cold and hot DT, which results in a smaller hot DT core with a transition region—a mixing layer at a temperature T^* ($T_p < T^* < T_{hc}$) with a mass density ρ^* ($\rho_{hc} < \rho^* < \rho_p$). Thus, $(\rho R)_{hs} = (\rho R)_{hc} + \rho^* h$, where the subscript "hc" denotes hot core and h the mixing width that is a function of the convergence ratio [5]. Hence, $1/(\rho R)_{hs} \approx (1 - \frac{\rho^* h}{(\rho R)_{hc}})/(\rho R)_{hc}$. Thus, the analytic expression for the ITF becomes

$$\mathrm{ITF} = \frac{3M_{\mathrm{pusher}}}{8\pi\psi(T_{\mathrm{ign}})}\left(1 - \frac{\rho^*}{\rho_{hc}}\frac{h}{R_{hc}}\right)^3\left(\frac{3\gamma_p - 1}{\gamma_p - 1}\right)^{-1} \times\left(\frac{3\gamma_p - 1}{\gamma_p/\epsilon_0}\right)^{-\frac{2\gamma_p}{\gamma_p - 1}} \eta^{\frac{3\gamma_p - 1}{\gamma_p - 1}} V_{\mathrm{imp}}^{\frac{6\gamma_p - 2}{\gamma_p - 1}}, \tag{14}$$

where

$$\psi(T_{\mathrm{ign}}) \equiv \left[\frac{\kappa(1+d)^2}{T_{\mathrm{ign}}(\mathrm{keV})^{2.5} d}\right]^3 \epsilon_{hs}\left(\frac{2N_A k T_{\mathrm{ign}}}{A_{\mathrm{DT}} P_0}\right)^2.$$

The ITF must be greater than 1 to achieve ignition at NIF.

The ITF derived here is from first principles and independent of any computational models. The advantage of an analytic expression over code simulations is that the analytic expression clearly displays the unique correlations among the design parameters in layers. The codes, however, cannot separate the physics impacts from the various parameters in a clear manner, although more physics and more nonlinear interrelationships may be included as compared to the analytic model. Our ITF is fundamentally different from the computationally based ITF. First, the temperature dependence of our derived ITF presents a more stringent condition for ignition than the current ITF, which does not take into account the ignition temperature of the hot fuel explicitly. Second, our ITF shows that ignition is much more sensitive to the peak implosion velocity and the pusher EOS than previously thought. For example, if the peak implosion velocity misses the required velocity threshold by 10%, then our ITF would drop 72% for $\gamma_p \simeq 5/3$ and 85% for $\gamma_p \simeq 4/3$, while the old ITF would only drop 57%. Also varying the pusher EOS from $\gamma_p \approx 3$ to $\gamma_p \approx 5/3$, alone, causes the ITF to fall at least a factor of 6. This implies that if the simulations correspond to a low-entropy adiabat of the pusher (e.g., $\gamma_p = 3$), then the calculated ITF would be at least six times the real ITF value in the experiments.

The stiffer behavior of the pusher in the simulations can be attributed to at least two sources: (1) a poor understanding of opacity and heat conduction in the cold DT [6], and inaccuracies in the cold DT EOS used in the codes and (2) the unmodeled presence of unexpected preheat or shock and reflected shocks in the pusher, possible chaotic mixing between cold and hot DT, and plasma effects [7]. Both sources would significantly alter the energy partition between the pusher and hot spot. This study suggests that a cold pusher with a high adiabat index and a hot spot with a low adiabat index would dramatically enhance the energy, mass, areal density, and pressure of the hot spot relative to the pusher and lead to higher thermonuclear reactivity. Certainly, implosion asymmetry [8] and the inevitable growth of instabilities at the interface between the pusher and the hot spot impose another challenge to the ignition, However, one key point we would like to make here is that for the current NIF capsule design, even if a perfect symmetry is maintained during implosion and even if all the NIF scaling laws and TN criterion are satisfied, the distance to achieving ignition at NIF still remains.

The authors are grateful to D. Clark, C. Cerjan, S. Haan, J. Nuckolls, and the LLNL NIC Team for valuable comments and sharing data and calculations, to J. Mercer-Smith for useful discussions, and to C. S. Carmer for help with the manuscript. This work was performed under the auspices of the US Department of Energy by the Los Alamos National Laboratory under Contract No. W-7405-ENG-36.

[1] S. W. Haan *et al.*, Phys. Plasmas **18**, 051001 (2011).

[2] W. K. Levedahl and J. D. Lindl, Nucl. Fusion **34**, 191 (1997); M. M. Basko and J. Johner, *ibid.* **38**, 1779 (1998); M. C. Herrmann, M. Tabak, and J. D. Lindl, *ibid.* **41**, 99 (2001); D. S. Clark, S. W. Hann, and J. D. Salmonson, Phys. Plasmas **15**, 056305 (2008); J. Meyer-Ter-Vehn, Nucl. Fusion **22**, 561 (1982); A. Kemp, J. Meyer-ter-Vehn, and S. Atzeni, Phys. Rev. Lett. **86**, 3336 (2001); M. M. Basko and J. Meyer-ter-Vehn, *ibid.* **88**, 244502 (2002).

[3] C. Cerjan (private communication); C. Cerjan, P. T. Springer, and S. M. Sepke, Phys. Plasmas **20**, 056319 (2013).

[4] D. Clark *et al.*, Phys. Plasmas **20**, 056318 (2013).

[5] K. O. Mikaelian, Phys. Rev. A **42**, 3400 (1990).

[6] D. E. Hanson *et al.*, Phys. Plasmas **18**, 082704 (2011); C. E. Starrett *et al.*, *ibid.* **19**, 102709 (2012).

[7] P. C. Amendt *et al.* (private communication).

[8] R. H. H. Scott *et al.*, Phys. Rev. Lett. **110**, 075001 (2013).